Quantum nonlinear dynamics of optomechanical systems in the strong-coupling regime

Machado, J. D.P.; Blanter, Ya M.

DOI
10.1103/PhysRevA.94.063835

Publication date
2016

Document Version
Final published version

Published in
Physical Review A: covering atomic, molecular, and optical physics and quantum information

Citation (APA)
Machado, J. D. P., & Blanter, Y. M. (2016). Quantum nonlinear dynamics of optomechanical systems in the strong-coupling regime. *Physical Review A: covering atomic, molecular, and optical physics and quantum information*, *94*(6), Article 063835. https://doi.org/10.1103/PhysRevA.94.063835

Quantum nonlinear dynamics of optomechanical systems in the strong-coupling regime

J. D. P. Machado and Ya. M. Blanter
Kavli Institute of Nanoscience, Delft University of Technology, Lorentzweg 1, 2628 CJ Delft, The Netherlands
(Received 6 July 2016; published 16 December 2016)

With an increasing coupling between light and mechanics, nonlinearities begin to play an important role in optomechanics. We solve the quantum dynamics of an optomechanical system in the multiphoton strong-coupling regime retaining nonlinear terms. This is achieved by performing a Schrieffer-Wolff transformation on the Hamiltonian including driving terms. The approach is valid away from the red- and blue-sideband drive. We show that the mechanical resonator displays self-sustained oscillations in regimes where the linear model predicts instabilities and that the amplitude of these oscillations is limited by the nonlinear terms. Related oscillations of the photon number are present due to frequency mixing of the shifted mechanical and cavity frequencies. This leads to additional peaks in the cavity's spectral density. Furthermore, we show that it is possible to create phonon states with sub-Poissonian statistics when the system is red detuned. This result is valid even with strong driving and with initial coherent states.

DOI: 10.1103/PhysRevA.94.063835

I. INTRODUCTION

By coupling light and mechanics, optomechanical systems enable control of light by mechanical motion and vice versa. This coupling of light to the modes of a mechanical resonator is often achieved via radiation pressure. Its nature is intrinsically nonlinear, but its strength is typically smaller than all other physical parameters [1], undermining the significance of nonlinear effects. The majority of the observed physical phenomena can be thus understood using a linear description.

The achievement of cooling a mechanical mode to its ground state [2,3] paves the way to state preparation, and it increased the interest in quantum effects in mechanical motion, specifically creation of nonclassical mechanical states. Such states can only be created in a nonlinear system, shifting the focus of attention to the single-photon strong-coupling (SPSC) regime, where quantum dynamics and properties have been analyzed theoretically. The exact solution for the isolated system was discovered [4,5]. Dissipation, noise, and the coherent drive have also been investigated by including them in the equations of motion and treating them as perturbations to the exact solution [6,7]. For this weak driving regime, it was found that mechanical states with sub-Poissonian statistics can be created in the SPSC regime. This conclusion was corroborated by numerical simulations [8–10]. Other works reported similar quantum states [11–13] over some parameter regions in the SPSC regime and signaled a connection to the self-sustained oscillations present in the nonlinear regime. Experimentally, the SPSC regime remains a challenge, though considerable progress has been made.

Higher single-photon coupling strengths were already obtained in a variety of setups where the single-photon coupling g_0 surpasses the mechanical frequency Ω [14] (or is close to it [15]). However, in these setups, the cavity linewidth κ exceeds the single-photon coupling, which prevents the development of nonclassical states [6]. Thus, in order to create truly quantum states, the coupling must be enhanced, which can be done by coherently driving the system. The drive enhances the single-photon coupling by a factor of $\sqrt{N_{\text{photons}}}$, which can go as high as 10^5 [16] and can place this effective coupling higher than the cavity linewidth and close to the magnitude of the mechanical frequency [3,16–18], making this multiphoton strong-coupling (MPSC) regime more experimentally relevant. At the MPSC regime, fluctuations are usually negligible, and linearizing the interaction is often sufficient to describe the behavior of the system. The resulting linear system can be solved, yielding instabilities for certain detunings. In the blue sideband, the instability is easily achieved even in the weak-coupling regime. When these instabilities occur, self-sustained oscillations of the mechanical resonator emerge. Such oscillations were already reported experimentally [19] and for intense drive powers, chaotic motion takes place [20]. To describe these phenomena, nonlinearities are essential, and in the absence of intrinsic nonlinearities, the nonlinear character of the interaction must be taken into account. The existent theoretical description of this regime with strong driving is mostly classical, but there has been recently a growing interest in its quantum counterpart. Nonlinear corrections to optomechanically induced transparency (OMIT) were obtained for this regime (through perturbation theory [21] and resorting to the Keldysh formalism approach [22]). The nonlinear interaction can also lead to parametric down-conversion between hybrid excitations of photons and phonons, the polaritons. This phenomenon occurring in the red sideband has also been studied [23,24].

In this article, we present a different approach to address the quantum dynamics of an optomechanical system that accounts for the nonlinearity of the interaction while considering strong driving. This approach is based on a Schrieffer-Wolff transformation [25] of the Hamiltonian and allows for an analytical solution. It is valid over a broad range of frequencies away from the red- and blue-detuned sidebands and for coupling strengths up to the mechanical frequency. It also enables us to evaluate quantum properties of the system and to derive its dynamics in a consistent way without any *a priori* ansatz. The results reveal the presence of self-sustained oscillations in the motion of the resonator and oscillations in the photon number arising from frequency mixing processes. These latter oscillations lead to the appearance of new peaks in the cavity's spectral density. If the cavity linewidth is small

enough such that the condition

$$2\frac{g_0^2}{\kappa\Omega} > 1 \tag{1}$$

is met, the photon statistics become distinguishable in the spectrum due to the effective Kerr nonlinearity. In this case, a sequence of peaks separated from each other by $2g_0^2\Omega$ appears in the cavity spectrum, whose height is proportional to $|\langle\psi|n\rangle|^2$, where $|\psi\rangle$ is the cavity state. Additionally, we show that it is possible to create phonon states with sub-Poissonian statistics when the system is red detuned. This result holds at the strong driving regime and even with initial coherent states.

In Sec. II, we present the Hamiltonian modeling this system and the unitary transformation performed to diagonalize the Hamiltonian up to η^2, where $\eta = g_0/\Omega$. This transformation retains the nonlinearity and is suitable for strong driving. At the end of the section, we evaluate the parameter region where the approach is valid. In Sec. III, we analyze the effects of thermal baths coupled to the system and derive the solutions for the equations of motion in the presence of dissipation and noise. With these solutions, the dynamics for the cavity and for the resonator are analyzed. In Sec. III A, the spectral density for the cavity field is computed and the existence of photon number oscillations is shown. The condition for the photon statistics to be observed in the cavity spectrum is also evaluated here. In Sec. III B, the emergence of self-sustained oscillations is shown, resorting to the derived solution for the mechanical resonator. The phonon statistics are also analyzed, revealing sub-Poissonian statistics in the red sideband for different initial states. We discuss the results in Sec. IV. Technical details are relegated to the appendixes.

II. THE MODEL

An optomechanical system can be modeled as two harmonic oscillators (the mechanical resonator and the cavity field) that couple through radiation pressure. This coupling is proportional to the field intensity and approximately linear in displacement. Including the driving term leads to the Hamiltonian [1]

$$\mathcal{H} = -\Delta a^\dagger a + \Omega b^\dagger b - g_0 a^\dagger a(b^\dagger + b) + \mathcal{E}(a^\dagger + a), \tag{2}$$

where Δ is the detuning of the driving laser from the cavity frequency ω_c, Ω is the mechanical frequency, g_0 is the optomechanical coupling, $\mathcal{E}$ is the driving strength, and a (b) represents the cavity's photon (phonon) annihilation operator in the frame rotating with the driving frequency ω_L.

In order to sweep away the direct influence of the driving term, a shift on the photon operator $a = A + \alpha$ is made, with α chosen such that no driving terms appear on the equations of motion. For a weakly interacting system, $\alpha \approx \mathcal{E}/(\Delta + i\kappa/2)$. With this shift, the operator A obeys the same commutation relations as a and represents the field displacements around the coherent component α produced by the driving laser. In the discussions ahead, the cavity states refer to the displaced states upon which A acts.

The Hamiltonian in Eq. (2) takes the form $\mathcal{H} = \mathcal{H}_0 - \eta V$, with $\eta = g_0/\Omega$ and

$$\begin{aligned} V = {} & \Omega[A^\dagger A(b^\dagger + b) + \alpha^* A(b + b^\dagger) \\ & + \alpha A^\dagger(b + b^\dagger) + |\alpha|^2(b + b^\dagger)]. \end{aligned} \tag{3}$$

For most experiments, the parameter η is typically of the order of 10^{-3} or even less [1]. By driving the system with a strong coherent source, the interaction is enhanced by a α factor and the effects of radiation pressure become visible. This regime where the coupling is enhanced by coherent light is the MPSC regime and the usual approach to deal with this regime is to consider only the interaction terms that were enhanced by α [the quadratic terms in Eq. (3)] and neglect the remaining ones (the nonlinear term). The outcome is a a linear system of equations for the fields, where dissipation and thermal noise can be added. This treatment is known to be sufficient to describe the basic features of an optomechanical system, such as laser cooling, optical spring effect, or the avoided crossing between the optical and the mechanical modes, and also predicts the existence of unstable regions with an effective negative damping. Yet, it is unable to describe the evolution of the system when the instability takes place, nor to account for the development of nontrivial quantum states. To do so, one must take into account the intrinsic nonlinearity of the interaction.

A. Schrieffer-Wolff transformation

As η is rather small, the coupling V can be seen as a perturbation, and one can perform a unitary transformation to obtain an effective Hamiltonian for which the effective interaction is even weaker. This effective Hamiltonian is given by $\mathcal{H}_{\text{eff}} = U\mathcal{H}U^\dagger$, with $U = e^{-\eta^2 T}e^{-\eta S}$, and where $\{S,T\}$ are anti-Hermitian operators. Performing the transformation leads to the effective Hamiltonian

$$\mathcal{H}_{\text{eff}} = \mathcal{H}_0 - \eta^2\left(\tfrac{1}{2}[S,V] + [T,\mathcal{H}_0]\right) + O(\eta^3), \tag{4}$$

by imposing the condition $[S,\mathcal{H}_0] = V$. This removal of the first-order dependence on η defines a Schrieffer-Wolff (SW) transformation. Choosing $\{S,T\}$ properly allows us to diagonalize the Hamiltonian up to η^2. To fulfill this condition, S and T must be

$$S = -|\alpha|^2 b + \frac{\alpha^*\Omega}{\Delta - \Omega}Ab - \frac{\alpha\Omega}{\Delta + \Omega}A^\dagger b - A^\dagger Ab - \text{H.c.}, \tag{5}$$

$$\begin{aligned} T = {} & d_{19}AA + d_{21}A^\dagger AA + d_{23}Abb + d_{25}A^\dagger bb \\ & + d_{27}Ab^\dagger b + d_{29}bb - \text{H.c.}, \end{aligned} \tag{6}$$

where H.c. stands for the Hermitian conjugate. The coefficients $\{d_j\}$ for the T operator are shown in Table I.

TABLE I. Coefficients for T.

d_{19}	$\frac{\Delta\alpha^* - \mathcal{E}}{2\Delta}d_{21} - \frac{\Omega^3}{2\Delta(\Delta^2 - \Omega^2)}(\alpha^*)^2$
d_{21}	$-\frac{\Omega(2\Omega^2 - \Delta^2)}{\Delta(\Delta^2 - \Omega^2)}\alpha^*$
d_{23}	$-\frac{\Delta\Omega}{2(\Delta - 2\Omega)(\Delta - \Omega)}\alpha^*$
d_{25}	$-\frac{\Delta\Omega}{2(\Delta + 2\Omega)(\Delta + \Omega)}\alpha$
d_{27}	$\frac{\Omega^2}{\Omega^2 - \Delta^2}\alpha^*$
d_{29}	$\frac{\Delta\Omega}{2(\Delta^2 - \Omega^2)}\lvert\alpha\rvert^2 + \frac{1}{2\Omega}[(\Delta\alpha - \mathcal{E})d_{23} + (\mathcal{E} - \Delta\alpha^*)d_{25}]$

The explicit form of the effective Hamiltonian is then

$$\mathcal{H}_{\rm eff} = -\bar{\delta}A^\dagger A + \eta^2\Omega(A^\dagger A)^2 + \tilde{\Omega}b^\dagger b, \tag{7}$$

and $\bar{\delta}$ and $\tilde{\Omega}$ are

$$\bar{\delta} = \Delta + 2\frac{g^2}{\Omega}\frac{2\Omega^2-\Delta^2}{\Delta^2-\Omega^2} + 4\eta^2{\rm Re}\{(\mathcal{E}-\Delta\alpha)d_{21}\}, \tag{8}$$

$$\tilde{\Omega} = \Omega - 2\frac{g^2}{\Omega}\frac{\Delta\Omega}{\Delta^2-\Omega^2} - 2\eta^2{\rm Re}\{(\mathcal{E}-\Delta\alpha)d_{27}\}, \tag{9}$$

with $g := g_0|\alpha|$. The Hamiltonian in Eq. (7) exhibits a Kerr nonlinearity for the photons (given by the $(A^\dagger A)^2$ term, similar to [6,7]), and the mechanical and cavity frequencies shifted due to the interaction [as seen from the effective detuning $\bar{\delta}$ at Eq. (8) and the effective mechanical frequency $\tilde{\Omega}$ at Eq. (9)]. It also presents the advantage of decoupling the photon sector from the phonon one, which simplifies the equations of motion.

B. Validity of the approach

So far, the only approximation considered was to disregard high-order terms (h.o.t.) in η. Although η is small, the h.o.t. contain powers of α, so they may become relevant for certain parameter values. In order to determine the validity region of our approach, we evaluate the h.o.t. and compare them with the expression for the effective Hamiltonian. The expression for the third-order terms is quite long, and it does not present any terms in common with the effective Hamiltonian. To properly evaluate its magnitude, one should be able at least to estimate the value of the field operators in order to assess their magnitude. This is a nontrivial matter, since the dynamics can make their value time dependent and their expressions are rather cumbersome. This can be surpassed by evaluating the fourth-order terms and compare the coefficients for the common terms. Comparing the ratio between the fourth-order coefficients [displayed at Eqs. (A2)–(A4) in Appendix A] and their counterparts in the effective Hamiltonian, we can determine the parameter region where the approach breaks down. This establishes a critical value $g_{\rm crit}$ for the coupling, at which h.o.t. begin to play a role. The $g_{\rm crit}$ is evaluated and shown in Fig. 1. The $g_{\rm crit}$ is roughly independent of the cavity linewidth, and it is always smaller than the mechanical frequency. It can be also seen from Fig. 1 that $g_{\rm crit} \to 0$ at $\Delta = \{0, \pm\Omega\}$, which excludes these detunings from the validity range, and the vicinity of these points can only be accessed by very small g.

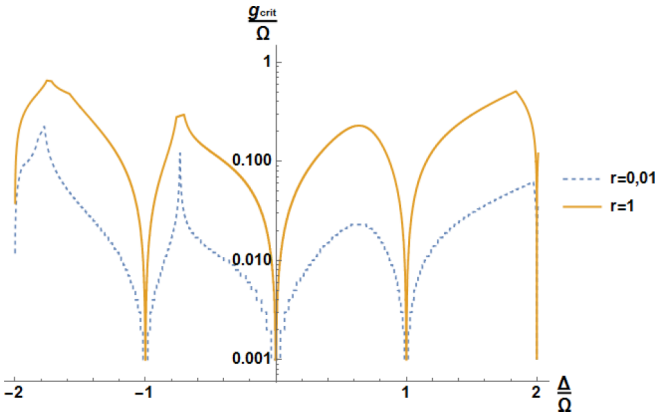

FIG. 1. Critical coupling at which the ratio between the higher-order terms and the lower ones is r. The points $\Delta = \{0, \pm\Omega\}$ are inaccessible.

III. DYNAMICS OF THE SYSTEM

To describe the physical system properly, we must take dissipation into account. This can be done by including a bath in the Hamiltonian as $\mathcal{H}_{\rm bath}$ of the form

$$\mathcal{H}_{\rm bath} = \sum_q \varpi_q c_q^\dagger c_q + \sum_q V_q c_q^\dagger(\alpha + A) + {\rm H.c.} + \sum_q \epsilon_q d_q^\dagger d_q + \sum_q M_q d_q^\dagger b + {\rm H.c.} \tag{10}$$

Performing the transformation $U = e^{-\eta^2 T}e^{-\eta S}$ to $\mathcal{H}_{\rm bath}$ and using the Markovian approximation leads to the dissipative and noise terms in the equations of motion. Although the transformation U leads to damping terms that couple the phonon and photon sectors or to additional nonlinear terms, these can be disregarded because they are off-resonant or have a lower magnitude in comparison to the remaining ones (see Appendix B). Resorting to Eq. (7), the photon and phonon sectors decouple in the equations of motion for the operators in the basis that diagonalizes the Hamiltonian up to η^2. The operators in this new basis $\{A_N, b_N\}$ are related to $\{A, b\}$ by

$$A_N = UAU^\dagger; \quad b_N = UbU^\dagger. \tag{11}$$

Considering the damping and noise terms, the equations of motion for the operators $\{A_N, b_N\}$ are

$$id_t A_N = \left(-\bar{\delta} - i\frac{\kappa}{2}\right)A_N + 2\eta^2\Omega A_N^\dagger A_N A_N, \tag{12}$$

$$id_t b_N = \left(\tilde{\Omega} - i\frac{\Gamma}{2}\right)b_N + f_b(t), \tag{13}$$

where κ and Γ are the photon and phonon decay rates, respectively, and where

$$\Gamma = 2\pi|M_q|^2\rho_b, \quad \kappa = 2\pi|V_q|^2\rho_a, \tag{14}$$

were taken as constants and ρ_j is the density of states for the bath j, and

$$f_b(t) = \sum_q M_q^* e^{-i\epsilon_q t}d_q(0). \tag{15}$$

The thermal noise source term f_b obeys $\langle f_b\rangle = 0$ and $\langle f_b(t)f_b(t')\rangle = \bar{n}_{th}\delta(t-t')$, while the thermal noise for the photons was neglected because their bath's temperature is null. The solutions for the equations of motion are straightforward to obtain and the time evolution for the operators $\{A_N, b_N\}$ is given by

$$A_N(t) = \Phi(t)A_N(0), \quad b_N(t) = \Theta(t)b_N(0) + F_b(t), \tag{16}$$

where

$$\Phi(t) = e^{(i\bar{\delta}-\kappa/2)t - 2i\frac{g_0^2}{\kappa\Omega}(e^{-\kappa t}-1)(A_N^\dagger A_N)(0)}, \tag{17}$$

$$\Theta(t) = e^{(-i\tilde{\Omega}t - \frac{\Gamma}{2})t}, \tag{18}$$

and

$$F(t) = \sum_q \frac{M_q^*}{\epsilon_q - \tilde{\Omega} + i\frac{\Gamma}{2}}[e^{-i\epsilon_q t} - \Theta(t)]d_q(0). \quad (19)$$

To evaluate physical observables, we express the operators in the original basis that represents the physical entities: $\{A,b\}$. A closed form for the representation of the operators in the original basis is impossible to obtain. Nevertheless, one can estimate the expressions at Eq. (11) by expanding U in powers of η and arrive at simple expressions relating the new basis and the original one.

From now on, we focus on the strong driving regime, defined by $|\alpha|^2 \gg \eta^{-1}\sqrt{N_b+1}$, where N_b is the average phonon number. This regime makes the effective interaction important. It also simplifies the expressions, as some terms of the time-evolution of the fields become negligible.

A. Cavity field

The time-evolution for the cavity field A in the strong driving regime can be found resorting to Eqs. (11) and (16), and it is given by

$$A(t) \approx \Upsilon_0(t) + \Upsilon_1(t)A(0) + \Upsilon_2(t)A^\dagger(0) + \Upsilon_5(t)(A^\dagger A)(0) + \Upsilon_6(t)(AA)(0) + \Upsilon_{10}(t)(A^\dagger AA)(0), \quad (20)$$

with

$$\Upsilon_0 = \frac{g^2}{\Omega}\left\{\frac{\alpha}{\Delta+\Omega}\Theta(t) + \frac{\alpha}{\Delta-\Omega}\Theta^*(t) + \frac{\alpha\Delta}{\Omega^2-\Delta^2}[\Phi(t)+1]\right\} + O(|\alpha|^{-1}), \quad (21)$$

$$\Upsilon_1 = \Phi(t) + \left[\frac{g^2}{(\Delta+\Omega)^2}\Theta(t) - \frac{g^2}{(\Delta-\Omega)^2}\Theta^*(t) + \frac{4\Delta\Omega g^2}{(\Delta^2-\Omega^2)^2}\Phi(t) + \frac{2g^2}{\Omega^2}\Phi(t)(1-\mathrm{Re}\{\Theta(t)\})\right] + O(|\alpha|^{-1}), \quad (22)$$

$$\Upsilon_2 = 2i\eta^2\left[2d_{19}^*\mathrm{Im}\{\Phi(t)\} + \frac{\alpha^2\Omega^2}{\Delta^2-\Omega^2}\mathrm{Im}\{\Theta(t)\}\right] + O(|\alpha|^{-1}), \quad (23)$$

$$\Upsilon_5 = \eta^2\left\{2d_{21}^*[e^{-\kappa t} - \Phi(t)] - \frac{\Omega}{\Delta-\Omega}\alpha[\Phi(t)\Theta(t) - \Theta^*(t)] - \frac{\Omega}{\Delta+\Omega}\alpha[\Phi(t)\Theta^*(t) - \Theta(t)]\right\}, \quad (24)$$

$$\Upsilon_6 \approx \eta^2\Phi(t)\left\{d_{21}[1-\Phi(t)] - \frac{\Delta\Omega\alpha^*}{\Delta^2-\Omega^2}[\Phi(t)+1] + \frac{\Omega\alpha^*}{\Delta-\Omega}\Theta^*(t) + \frac{\Omega\alpha^*}{\Delta+\Omega}\Theta(t)\right\}, \quad (25)$$

$$\Upsilon_{10} = \eta^2\Phi(t)[\Theta^*(t) - \Theta(t)]. \quad (26)$$

The terms in Eq. (20) are the surviving terms in the strong driving limit. The corrections to this solution when the strong driving condition is not satisfied are presented in Appendix C.

With Eq. (20), the statistics for the cavity field can be evaluated. Due to the strong coherent driving, the cavity field acquires a large coherent component, but the time evolution depends on higher moments of the initial statistics of the cavity state. Thus, the state must be carefully evaluated. The state for which operator order is most relevant is the $|0\rangle$ state. For this state, the second-order correlation function takes the value

$$g^{(2)} \approx 1 + 4\eta^2\left(\frac{g}{\Omega}\right)^2 \approx 1 \quad (27)$$

in the strong driving limit. Evaluating any other correlation function would render a similar result, i.e., the corresponding value for a coherent state. As the photon state can be obtained through evaluation of all correlation functions, the cavity field must be in a coherent state at all times. It must be also noted that any difference between the average values of operators with a different order will be of the same order of magnitude as the previously disregarded terms. This classicality stems from the strong coherent driving, which imposes a large coherent state for the cavity field.

From the time dependence of $\{\Upsilon_i\}$, it can be seen that the time evolution of the cavity field oscillates with frequencies which are combinations of the cavity, the laser, and the mechanical frequencies. The focus of attention is commonly towards the cavity frequency and the sidebands around the laser frequency [1]. In the MPSC regime, additional frequencies arise, such as sidebands around the cavity frequency and frequency mixing of the cavity and laser frequencies. These are signatures of the nonlinear interaction. It can be also seen from Eq. (17) that the dependence of $\Phi(t)$ with the photon number implies that the spectral density exhibits a peak for each excitation number. To first order in η, $A_N = A + O(\eta)$, and so the time evolution for the cavity field presents the component

$$\Phi(t)|\psi\rangle \approx \sum_n e^{(i\bar{\delta}-\kappa/2)t - 2i\frac{g_0^2}{\kappa\Omega}(e^{-\kappa t}-1)(A^\dagger A)}c_n|n\rangle \approx \sum_n e^{i(\bar{\delta}-2\frac{g_0^2}{\Omega}n)t}c_n|n\rangle \quad (28)$$

in the limit $\kappa \to 0$. Equation (28) presents a different oscillating frequency for each photon number. Therefore, the light spectrum is sensitive to the photon statistics due to the Kerr nonlinearity and each peak is separated from each other by $2g_0^2/\Omega$. To be able to distinguish between consecutive peaks and so evaluate the statistics of the field, the condition

$$2\frac{g_0^2}{\kappa\Omega} \gg 1 \quad (29)$$

is required. Thus, this ratio corresponds to a granularity parameter, which determines the possibility to observe individual photons. However, for current experimental parameters, this value is quite small. For large coherent states (which can be created resorting to strong driving), the distribution of the peaks' heights follows a Poissonian distribution. For this case, the inability to resolve between consecutive peaks leads to an apparent increase of the linewidth by g^2/Ω due to the variance of the distribution. As this typically does not constitute a

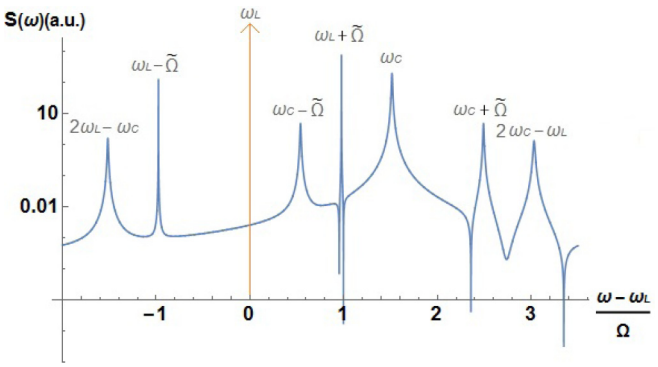

FIG. 2. Noise power spectral density of the cavity field for $\Delta = -1.5\Omega$, $g = 0.1\Omega$, and $\kappa = 0.01\Omega$. The nonlinear interaction generates sidebands around the cavity frequency and other frequency mixing processes between the cavity frequency and the laser frequency (such as the peak at $2\omega_c - \omega_L$).

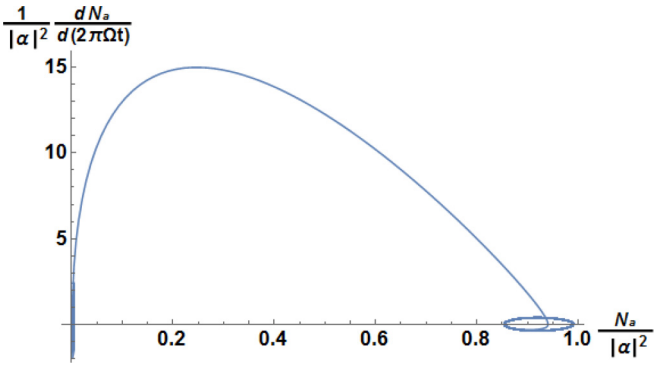

FIG. 3. Photon number time evolution for $\Delta = -1.8\Omega$, $g = 0.3\Omega$, and $\kappa = 10\Omega$. The system converges to an ellipse in $(N_a, d_t N_a)$ phase space, which represents an oscillation of the photon number $\langle a^\dagger a\rangle$.

significant increase in the linewidth, we can approximate $A_N^\dagger A_N$ in the exponential of Eq. (28) by its average value.

Evaluating the noise power spectral density for the cavity field, one can see the appearance of the new frequencies originated by the nonlinear interaction. This is given by

$$S(\omega) = \frac{1}{2}\int dt\,\langle \mathcal{A}(t)\mathcal{A}(0) + \mathcal{A}(0)\mathcal{A}(t)\rangle e^{i\omega t}, \tag{30}$$

where $\mathcal{A} = A^\dagger + A$ is the amplitude for the cavity field. In order for the frequencies to be visible, one must be in the resolved sideband regime ($\Omega \gg \kappa$) and choose a proper detuning such that the peaks do not overlap. Choosing the initial cavity state $|-\alpha\rangle$, i.e., the vacuum state for the original undisplaced cavity operator, we obtain the spectral density presented in Fig. 2. Note that multiple frequencies were reported in [14,20], but the underlying mechanisms are different from the one discussed here.

As the coupling increases, so does the amplitude of the oscillations at these frequencies, and the oscillations become prominent. They are responsible for the appearance of oscillations in the photon number. The time evolution of the photon number can be described better by representing the trajectory in the $(N_a, d_t N_a)$ phase space. By doing so, one can visualize the whole time evolution and identify the limit cycles. Evaluating the time evolution of the photon number $\langle a^\dagger a\rangle(t)$ for the same initial state, one can see in Fig. 3 that the motion of the system converges to an ellipse in the $(N_a, d_t N_a)$ phase space, representing the oscillation in the photon number.

B. Mechanical resonator

Photon number oscillations are known to be connected to self-sustained oscillations of the mechanical resonator [20], and we can now address the time evolution for the displacement of the resonator in the nonlinear regime without any *a priori* assumption. By the same procedure employed for the cavity case, the time evolution of $b(t)$ in the strong driving regime is found to be

$$b(t) \approx \Xi_0(t) + \Xi_4(t)b(0) + \Xi_5(t)b^\dagger(0) + \Xi_1(t)A(0) + \Xi_2(t)A^\dagger(0) + \Xi_3(t)A^\dagger(0)A(0), \tag{31}$$

with

$$\Xi_0(t) = -\frac{g}{\Omega}|\alpha|[1-\Theta(t)] + \left[1 + \frac{2g^2\Delta\Omega}{(\Delta^2-\Omega^2)^2}\right]F_b(t) + 2\eta^2 d_{29}^* F_b^\dagger(t), \tag{32}$$

$$\Xi_1(t) = -\eta\frac{\Omega}{\Delta+\Omega}\alpha^*[\Phi(t)-\Theta(t)] + O(\eta^2), \tag{33}$$

$$\Xi_2(t) = \eta\frac{\Omega}{\Delta-\Omega}\alpha[\Phi^*(t)-\Theta(t)] + O(\eta^2), \tag{34}$$

$$\Xi_3(t) = \eta[\Theta(t) - e^{-kt}], \tag{35}$$

$$\Xi_4(t) = \Theta(t) + \frac{g^2}{(\Delta-\Omega)^2}[\Theta(t)-\Phi^*(t)] + \frac{g^2}{(\Delta-\Omega)^2}[\Phi(t)-\Theta(t)], \tag{36}$$

$$\Xi_5(t) = 2\eta^2 d_{29}^*[\Theta^*(t)-\Theta(t)] + \frac{g^2}{\Omega^2-\Delta^2}[\Phi^*(t)-\Phi^*(t)]. \tag{37}$$

It is known that in the linear model, for some parameters, a negative effective damping occurs, leading to an instability. This instability can arise in the blue sideband, even in the weak-coupling regime. From Eq. (31), the time evolution for the displacement of the resonator $\langle x(t)\rangle = \langle b(t) + b^\dagger(t)\rangle$ is easily obtained, and with it, the complete dynamics past the initial instability can be evaluated. Considering the initial state $|-\alpha;0\rangle$, the displacement for the resonator is given by

$$\langle x(t)\rangle \approx \frac{2g}{\Omega}|\alpha|\left\{\frac{2\Delta^2}{\Delta^2-\Omega^2}e^{-\frac{\Gamma}{2}t}\cos(\tilde{\Omega}t) - 1 - e^{-\kappa t} - \frac{2\Omega^2}{\Delta^2-\Omega^2}e^{-\frac{\kappa}{2}t}\cos\left[\bar{\delta}t - \frac{g^2}{\kappa\Omega}(e^{-\kappa t}-1)\right]\right\}. \tag{38}$$

It is seen in Fig. 4 that after the initial growth of the displacement (lasting k^{-1}), the resonator starts to develop long-lasting oscillations. This motion of the mechanical resonator is a characteristic of self-sustained oscillations, which can be identified by the elliptic shape drawn by the motion in phase space. The origin of these oscillations can be found in the expression for $\langle x(t)\rangle$ and it arises from destructive interference

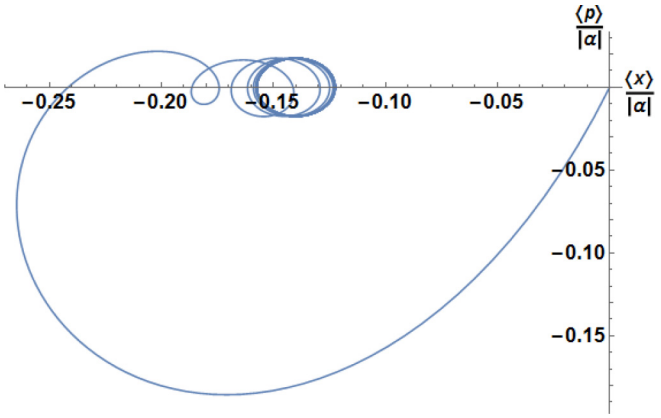

FIG. 4. Time evolution of the resonator in the (x,p) phase space for $\Delta = 0{,}6\Omega$, $\kappa = \Omega$, $g = 0{,}07\Omega$, and $\Gamma = 0$. For these parameters, the linear model predicts an instability. The initial growth of the displacement converges to an ellipse in phase space, which represents self-sustained oscillations.

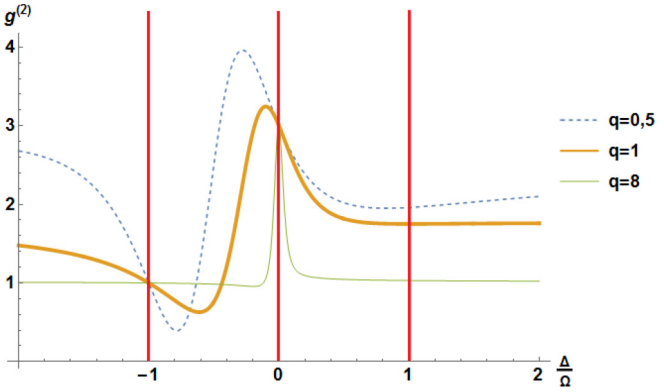

FIG. 5. $g^{(2)}(t_m^*)$ as a function of detuning for the initial state $|q;0\rangle$, with the coherent photon state $|q\rangle = \{|0.5\rangle, |1\rangle, |8\rangle\}$. The mechanical state exhibits sub(super)-Poissonian statistics when red (blue) detuned for initial states with $|q| \leqslant 1$ (thick and dashed lines). As the coherent states become larger, the effect vanishes (as seen from the thin line corresponding to $q = 8$). It is assumed that the transient time κ^{-1} has passed. The vertical thick lines delimit the regions where the approach does not hold.

between two oscillations with different decay rates, as seen from Eq. (38).

With Eq. (31), the phonon statistics can be computed. In the strong driving regime, the mechanical resonator acquires a massive coherent state with a thermal noise component (as can be seen from Ξ_0), and the statistics of the mechanical resonator can be evaluated via the same procedure performed for the cavity field. The magnitude of Ξ_0 implies a displaced thermal state (a coherent state with the quadratures' uncertainties broadened by thermal noise) for the phonons and so the resonator does not have unique quantum properties. However, the dominant term Ξ_0 vanishes periodically every $t_m^* = \frac{2\pi m}{\Omega}$, in the limit $\Gamma \to 0$. This allows a short time window ($\Delta\tau \propto |\alpha|^{-1}$), in which the resonator is able to depart from a displaced thermal state. If the resonator starts in the ground state, the coupling does not play a role in the state developed at t_m^*, and after the transient time κ^{-1}, the state is determined solely by the detuning and the initial cavity state. It must be noted that thermal noise does not affect this result. The contributions for $F(t)$ come mainly from the bath degrees of freedom within a narrow window (of width $\sim \Gamma$) of frequencies around $\tilde{\Omega}$, which results in $F(t = t_m^*) = 0$ in the limit $\Gamma \to 0$. To characterize the resonator state, we employ $g^{(2)}$. For the initial state $|q;0\rangle$, where q is the amplitude of a coherent state, and using the notation $X_j = \Xi_j(t_m^*)$, $g^{(2)}(t_m^*)$ is given by

$$g^{(2)}(t_m^*) = 1 + \frac{1}{(N_b)^2}\{|X_2|^2[|X_2|^2(1+2|q^2|) + |X_1|^2(1+6|q|^2)] + (2|X_1|^2 + 6|X_2|^2) \times \mathrm{Re}\{X_1 X_2^* q^2\}\}, \tag{39}$$

with

$$N_b = |qX_1|^2 + |X_2|^2(|q|^2+1) + 2\mathrm{Re}\{X_1 X_2^* q^2\}. \tag{40}$$

For this type of initial state, sub-Poissonian statistics are visible when red detuned (see Fig. 5) and when $|q| \leqslant 1$. As the amplitude of the initial coherent state increases, this characteristic starts to disappear.

Thus, it is possible for the phonon state to have sub-Poissonian statistics at the particular times t_m^* provided that it has a sufficiently high mechanical quality factor. This is possible if the initial state is a coherent state with a low average photon number and the mechanical resonator is in the ground state, but it is not restricted to these initial states. Yet, it is remarkable that there is a possibility to create states with sub-Poissonian statistics starting with coherent states and driving the system with a strong coherent drive. It is also interesting to see how deviations from the ground state and different initial states affect this result. Let us now consider the initial state $|1;\beta\rangle$.The second-order coherence function is now given by

$$g^{(2)}(t_m^*) = 1 + \frac{1}{(\tilde{N}_b)^2}[|X_2|^2(5|X_1|^2 + 2|X_2|^2) - |X_1|^4 + 2|\beta X_4|^2(|X_1|^2 + 2|X_2|^2) + 6\mathrm{Re}\{X_1^* X_2^* (\beta X_4)^2\}], \tag{41}$$

with

$$\tilde{N}_b(t_m^*) = |X_1|^2 + 2|X_2|^2 + |\beta X_4|^2. \tag{42}$$

It can be seen from Fig. 6 that the mechanical resonator also displays sub-Poissonian statistics when the system is red detuned for different initial states. It also illustrates the importance of starting at the ground state. If the initial mechanical coherent state has a high average number of phonons (i.e., $|\beta|^2 > \frac{g}{\Omega}$), the sub-Poissonian nature of the state begins to disappear, and the initial mechanical state reemerges at t_m^*. Note that the parameter region where the approach is not valid in Fig. 6 is broader because we no longer consider only the ground state for the phonons. The phonon state has now an initial coherent component β that competes with the Fock state from the cavity, which has an associated relative weight of g/Ω. Thus, for the states and the coupling g chosen, the approach does not allow to go closer to the

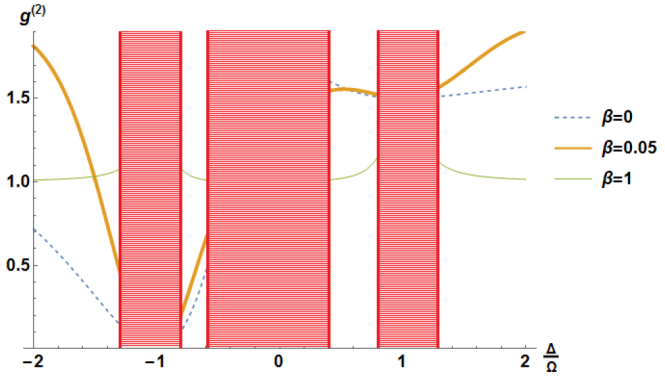

FIG. 6. $g^{(2)}(t_m^*)$ as a function of detuning for $g = 0.05$ and for the initial state $|1;\beta\rangle$. For these conditions, the mechanical resonator also exhibits sub-Poissonian statistics when the system is red detuned (dashed and thick lines). As the average phonon number $|\beta|^2$ increases, this feature starts to vanish, and coherent characteristics prevail (as seen from the thin line). The vertical shaded regions indicate where the validity breaks down.

detunings $\Delta = \{0, \pm\Omega\}$. Yet, the sub-Poissonian nature of the mechanical state is still visible in Fig. 6.

IV. CONCLUSION

Summarizing, we have shown that resorting to a Schrieffer-Wolff transformation, it is possible to obtain analytical solutions for the quantum dynamics of a strongly driven optomechanical system when the nonlinear interaction plays an important role. With this approach, the time evolution for the cavity and mechanical fields were obtained using an operator description, which enables us to evaluate their quantum properties.

The solutions show that the mechanical resonator develops self-sustained oscillations for parameter regions where the linear model predicts an instability. Thus, the nonlinear interaction limits the growth produced by a negative effective damping. Similar oscillations are also present in the photon number. Their origin is the existence of distinct frequencies in the cavity field, as revealed by the noise power spectral density. The spectral density also reveals the existence of frequency mixing between cavity, mechanical, and laser frequencies. Furthermore, if the condition

$$2\frac{g_0^2}{\kappa\Omega} > 1 \tag{43}$$

is satisfied, the photon statistics appear in the spectrum due to the effective Kerr nonlinearity. We have also shown that it is possible to create phonon states with sub-Poissonian statistics if the system is red detuned. Sub-Poissonian statistics for the distribution of the excitation number are only possible if the P distribution representing the state has negative values over any region in phase space. The fact that the P distribution presents negative regions implies that it is not a classical probability distribution and that we are in the presence of nontrivial quantum states. This result holds even in the strong driving regime and with initial (small) coherent states.

ACKNOWLEDGMENTS

This work was supported by the Dutch Science Foundation (NWO/FOM).

APPENDIX A: VALIDITY OF THE SW TRANSFORMATION

The unitary transformation $U = e^{-\eta^2 T} e^{-\eta S}$, with S and T defined by Eqs. (5) and (6), transforms the Hamiltonian in Eq. (2) into a Hamiltonian with the form

$$\begin{aligned}\mathcal{H}_{\rm eff} = \mathcal{H}_0 &+ \tfrac{1}{2}\eta^2[S,V] - \eta^2[T,\mathcal{H}_0] - \tfrac{1}{3}\eta^3[S,[S,V]] \\ &+ \tfrac{1}{8}\eta^4[S,[S,[S,V]]] - \tfrac{1}{2}\eta^4[T,[S,V]] \\ &+ \tfrac{1}{2}\eta^4[T,[T,\mathcal{H}_0]] + O(\eta^4).\end{aligned} \tag{A1}$$

We chose $\{S,T\}$ such that the Hamiltonian is diagonal up to η^2 and disregarded the higher-order terms in η. For this procedure to be valid, the disregarded terms must be smaller than the terms at Eq. (7). Thus, to delimit the validity region, the h.o.t. must be evaluated. The third-order contributions do not have any terms in common with the effective Hamiltonian, which makes it hard to assess. Therefore, we turn to the fourth-order terms containing common elements. The relevant terms of $[T,[T,\mathcal{H}_0]]$ are

$$\begin{aligned}&[T,[T,\mathcal{H}_0]] \\ &\to -6\Delta|d_{21}|^2(A^\dagger A)^2 \\ &\quad + [-16\Delta|d_{19}|^2 + 16\mathrm{Re}\{d_{19}d_{21}^*(\Delta\alpha - \mathcal{E})\}]A^\dagger A \\ &\quad + [16\Omega|d_{29}|^2 + 4\mathrm{Re}\{d_{27}d_{19}^*(\mathcal{E} - \Delta\alpha^*)\} \\ &\quad + 8\mathrm{Re}\{(\mathcal{E} - \Delta\alpha^*)d_{23}^* + (\Delta\alpha - \mathcal{E})d_{25}^*\}]b^\dagger b,\end{aligned} \tag{A2}$$

while the ones of $[T,[S,V]]$ are

$$\begin{aligned}&[T,[S,V]] \\ &\to 12\frac{2\Omega^2 - \Delta^2}{\Delta^2 - \Omega^2}d_{21}\alpha(A^\dagger A)^2 \\ &\quad + \left[4|\alpha|^2\frac{2\Omega^2 - \Delta^2}{\Delta^2 - \Omega^2}d_{27}\alpha + |\alpha|^2\frac{16\Delta\Omega}{\Delta^2 - \Omega^2}\mathrm{Re}\{d_{29}\}\right]b^\dagger b \\ &\quad + \left[\frac{16\Omega^2}{\Delta^2 - \Omega^2}\mathrm{Re}\{d_{19}\alpha^2\} - 8|\alpha|^2\frac{2\Omega^2 - \Delta^2}{\Delta^2 - \Omega^2}d_{21}\alpha\right]A^\dagger A,\end{aligned} \tag{A3}$$

and finally $[S,[S,[S,V]]]$ is

$$\begin{aligned}&[S,[S,[S,V]]] \\ &\to -128|\alpha|^4\frac{\Delta\Omega^3}{(\Delta^2 - \Omega^2)^2}A^\dagger A \\ &\quad - 8|\alpha|^2\left[11\frac{\Delta\Omega^3}{(\Delta^2 - \Omega^2)^2} + \frac{\Delta\Omega}{\Delta^2 - \Omega^2}\right](A^\dagger A)^2 \\ &\quad + 8|\alpha|^4\left[\frac{3\Omega^2}{\Delta^2 - \Omega^2} - 5\frac{(\Delta^2 + \Omega^2)\Omega^2}{(\Delta^2 - \Omega^2)^2}\right]b^\dagger b.\end{aligned} \tag{A4}$$

Comparing the coefficients in Eqs. (A2)–(A4) with the coefficients in Eq. (7) enables us to determine a region where the h.o.t. start to become important and where the approach is no longer valid. This is shown in Fig. 1. This

prohibited parameter region does not come from the form of the transformation chosen. The transformation $e^{-\eta S}$ is the most simple and necessary transformation to obtain a Schrieffer-Wolff transformation. Considering only its contribution, a similar parameter restriction is found because h.o.t. of S diverge close to $\Delta = \pm\Omega$ more rapidly than the corresponding ones in Eq. (7). Thus, we have an unsurpassable limit for the validity of any transformation of this kind.

Analyzing separately the contribution of each term to the critical g, one finds that the biggest change as g increases is in the nonlinear term $(A^\dagger A)^2$. This suggests that nonlinear effects may dominate the physics beyond the strong-coupling regime.

APPENDIX B: FUNCTIONAL FORM OF DISSIPATION

Let us consider two distinct thermal baths composed of harmonic oscillators for the photons and phonons. The Hamiltonian modeling the thermal baths and their interaction with the system is given by $\mathcal{H}_{\text{bath}}$, which has the form of Eq. (10). Performing the unitary transformation $U = e^{-\eta^2 T} e^{-\eta S}$ on the bath Hamiltonian $\mathcal{H}_{\text{bath}}$, the time evolution for the bath operators is given by

$$c_q(t) = e^{-i\varpi_q t}c_q(0) - iV_q\int_0^t e^{i(t'-t)\varpi_q}\Big\{\alpha + A(t') - \eta[S,A] - \eta^2[T,A] + \frac{1}{2}\eta^2[S,[S,A]] + O(\eta^3)\Big\}dt', \tag{B1}$$

$$d_q(t) = e^{-i\epsilon_q t}d_q(0) - iM_q\int_0^t e^{i(t'-t)\epsilon_q}(b(t') - \eta[S,b] - \eta^2[T,b] + \frac{1}{2}\eta^2[S,[S,b]] + O(\eta^3))dt', \tag{B2}$$

with

$$[S,A] = \frac{\Omega}{\Delta-\Omega}\alpha b^\dagger + \frac{\Omega}{\Delta+\Omega}\alpha b + Ab - Ab^\dagger, \tag{B3}$$

$$[S,b] = -|\alpha|^2 + \frac{\Omega}{\Delta-\Omega}\alpha A^\dagger - \frac{\Omega}{\Delta+\Omega}\alpha^* A - A^\dagger A, \tag{B4}$$

$$[S,[S,A]] \approx \frac{2|\alpha|^2\Delta\Omega}{\Omega^2-\Delta^2}\alpha + \frac{4|\alpha|^2\Delta\Omega^3}{(\Delta^2-\Omega^2)^2}A - \frac{2\alpha^*\Delta\Omega}{\Delta^2-\Omega^2}AA + \frac{\alpha\Omega}{\Delta+\Omega}bb - \frac{\alpha\Omega}{\Delta-\Omega}b^\dagger b^\dagger + \frac{2\alpha\Omega^2}{\Delta^2-\Omega^2}b^\dagger b - 2Ab^\dagger b + Abb + Ab^\dagger b^\dagger, \tag{B5}$$

$$[S,[S,b]] = \frac{4|\alpha|^2\Delta\Omega^3}{(\Delta^2-\Omega^2)^2}b - \frac{2\alpha\Delta\Omega}{\Delta^2-\Omega^2}A^\dagger b - \frac{2\alpha^*\Delta\Omega}{\Delta^2-\Omega^2}Ab, \tag{B6}$$

$$[T,A] = 2d_{19}^* A^\dagger - d_{21}AA + 2d_{21}^* A^\dagger A + d_{23}^* b^\dagger b^\dagger - d_{25}bb + d_{27}^* b^\dagger b, \tag{B7}$$

$$[T,b] = 2d_{23}^* A^\dagger b^\dagger + 2d_{25}^* Ab^\dagger - d_{27}Ab + d_{27}^* A^\dagger b + 2d_{29}^* b^\dagger. \tag{B8}$$

Using the Markovian approximation, the equations of motion for the system's operators become

$$id_t b = \left(\tilde{\Omega} - i\frac{\Gamma}{2}\right)b + i\frac{\Gamma}{2}\eta[S,b] + i\frac{\Gamma}{2}\eta^2\left([T,b] - \frac{1}{2}[S,[S,b]]\right) + O(\eta^3), \tag{B9}$$

$$id_t A = -\tilde{\delta}(A+\alpha) + \mathcal{E} - i\frac{\kappa}{2}(\alpha + A) + i\frac{\kappa}{2}\eta[S,A] - i\frac{\kappa}{2}\eta^2\left(\frac{1}{2}[S,[S,A]] - [T,A]\right). \tag{B10}$$

We can determine the value of α by enforcing the driving component to vanish in the equations of motion. This leads to the following equation for α:

$$\mathcal{E} = \left[\Delta\left(1 - \frac{g^2}{\Omega^2}\frac{2\Omega^2-\Delta^2}{\Delta^2-\Omega^2}\right) + i\frac{\kappa}{2}\left(1 + \frac{g^2\Delta\Omega}{\Omega^2-\Delta^2}\right)\right]\alpha + 2\eta^2[(\Delta\alpha^* - \mathcal{E})d_{19}^*]. \tag{B11}$$

It should be noted that Eq. (B11) already takes into account the change on the intracavity population originated by the cavity frequency shift caused by the interaction. Although α can be obtained from Eq. (B11) for any set of parameters, the relevant quantity for the system is g. Thus, we shall use g as the parameter of the system and determine $\mathcal{E}$ or the phase of α only when deemed necessary.

The introduction of dissipation couples the two sectors once again and introduces additional nonlinear terms. The terms that lack an associated α factor have a magnitude smaller than the others and become negligible in the strong driving regime. The remaining ones containing an α factor could play an important role, but they are only resonant around $\Delta = \pm\Omega$, where the approach is no longer valid. Just like in the sections where the validity is assessed, we shall evaluate in a similar manner the critical coupling $\tilde{g}_{\text{crit}}$ at which the corrections to damping become relevant.

Comparing the $\tilde{g}_{\text{crit}}$ from the corrections to the damping to the g_{crit} of the disregarded high-order terms, we find from Fig. 7 that the critical coupling for the damping corrections is always higher than the h.o.t. As g must be always smaller

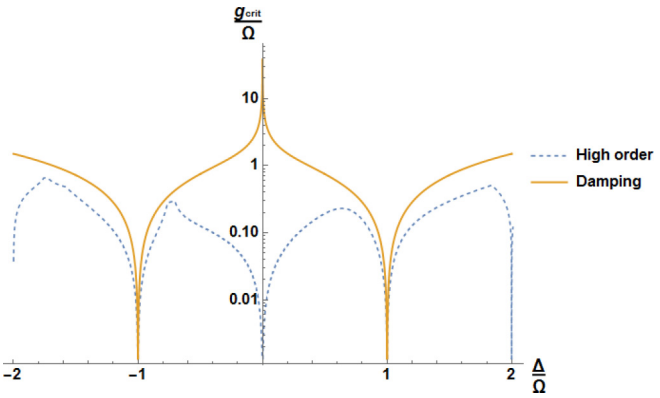

FIG. 7. Critical coupling at which high-order terms (dashed line) and corrections to the damping (thick line) begin to play a role. Since corrections from the high-order terms occur at lower coupling values than corrections to the damping, the last ones can be disregarded.

than Ω and we cannot be close to $\Delta = \pm\Omega$ for the approach to be valid, the contribution of the corrections to damping can be neglected.

APPENDIX C: DYNAMICS BEYOND THE STRONG DRIVING LIMIT

By expanding U in powers of η, we can obtain the dynamics of the system. The time-evolution of any operator O in the original basis is then

$$O = O_N + \eta[S, O_N] + \eta^2[T, O_N] + \tfrac{1}{2}\eta^2[S,[S, O_N]] + O(\eta^3). \tag{C1}$$

We can now compute the complete time-evolution for the cavity field. Because $\Phi(t)$ is an operator, one must take into account the commutation relations. Namely,

$$\Phi(t)A_N(0) = A_N(0)\Phi(t)e^{2i\eta^2\frac{\Omega}{\kappa}(e^{-\kappa t}-1)}. \tag{C2}$$

As η is very small for the case considered, this phase shift is negligible. The complete time evolution for the cavity field is found to be

$$\begin{aligned} A(t) = {} & \Upsilon_0 + \Upsilon_1 A(0) + \Upsilon_2 A^\dagger(0) + \Upsilon_3 b(0) + \Upsilon_4 b^\dagger(0) \\ & + \Upsilon_5 A^\dagger(0)A(0) + \Upsilon_6 A(0)A(0) + \Upsilon_7 b^\dagger(0)b(0) \\ & + \Upsilon_8 b(0)b(0) + \Upsilon_9 b^\dagger(0)b^\dagger(0) + \Upsilon_{10} A^\dagger(0)A(0)A(0) \\ & + \Upsilon_{11} A(0)b(0) + \Upsilon_{12} A(0)b^\dagger(0) + \Upsilon_{13} A(0)b(0)b(0) \\ & + \Upsilon_{14} a(0)b^\dagger(0)b(0) + \Upsilon_{15} A(0)b^\dagger(0)b^\dagger(0) + O(\eta^3), \end{aligned} \tag{C3}$$

with Υ_j from Eqs. (21)–(26) and the corrections

$$\begin{aligned} \Upsilon_0 \approx {} & \frac{g^2}{\Omega}\alpha\left\{\frac{1}{\Omega-\Delta}\left[\frac{1}{2}\Phi(t) - \Theta^*(t) + \frac{1}{2}\right] + \frac{1}{\Delta+\Omega}\left[\Theta(t) - \frac{1}{2}\Phi(t) - \frac{1}{2}\right]\right\} + 2\eta^2 d_{29}^* F^\dagger(t) \\ & + \eta\left[\frac{\Omega\alpha}{\Delta-\Omega}F^\dagger(t) - \frac{\Omega\alpha}{\Delta+\Omega}F(t)\right] + \frac{1}{2}\eta^2\left[\frac{\Omega\alpha}{\Delta+\Omega}(FF)(t) - \frac{\Omega\alpha}{\Delta-\Omega}(F^\dagger F^\dagger)(t) + \frac{2\alpha\Omega^2}{\Delta^2-\Omega^2}(F^\dagger F)(t)\right], \end{aligned} \tag{C4}$$

$$\begin{aligned} \Upsilon_1 \approx {} & \Phi(t) + \frac{g^2}{\Omega^2}\left\{\frac{\Omega^2}{(\Delta-\Omega)^2}[\Phi(t) - \Theta^*(t)] - \frac{\Omega^2}{(\Delta+\Omega)^2}[\Phi(t) - \Theta(t)] + \Phi(t)[2 - \Theta(t) - \Theta^*(t)]\right\} \\ & + \eta\Phi(t)[F(t) - F^\dagger(t)] + \eta^2\Phi(t)\left[-(F^\dagger F)(t) + \frac{1}{2}(FF + F^\dagger F^\dagger)(t) + 2d_{25}^* F^\dagger(t) - d_{27}F(t)\right], \end{aligned} \tag{C5}$$

$$\Upsilon_2 = -\eta^2\left\{2d_{19}^*[\Phi^*(t) - \Phi(t)] + \frac{\alpha^2\Omega^2}{\Delta^2-\Omega^2}[\Theta^*(t) - \Theta(t)]\right\}\eta^2\Phi^*(t)[2d_{23}^* F^\dagger(t) + d_{27}^* F(t)], \tag{C6}$$

$$\Upsilon_3 = \eta\frac{\Omega}{\Delta+\Omega}\alpha[\Theta(t) - \Phi(t)] + \eta^2\frac{\Omega\alpha}{\Delta+\Omega}\left\{\Theta(t)\left[F(t) + \frac{\Omega}{\Delta-\Omega}F^\dagger(t)\right] + \Phi(t)[F(t) - F^\dagger(t)]\right\}, \tag{C7}$$

$$\Upsilon_4 = \eta\frac{\Omega}{\Delta-\Omega}\alpha[\Theta^*(t) - \Phi(t)] - \eta^2\frac{\Omega\alpha}{\Delta-\Omega}\left\{\Theta^*(t)\left[F^\dagger(t) - \frac{\Omega}{\Delta+\Omega}F^\dagger(t)\right] - \Phi(t)[F(t) - F^\dagger(t)]\right\}, \tag{C8}$$

$$\Upsilon_7 = \eta^2\left\{d_{27}^*[e^{-\Gamma t} - \Phi(t)] - \frac{\Omega}{\Delta-\Omega}\alpha\left[\Theta(t)\Phi(t) - \frac{1}{2}e^{-\Gamma t} - \frac{1}{2}\Phi(t)\right] + \frac{\Omega}{\Delta+\Omega}\alpha\left[\Theta^*(t)\Phi(t) - \frac{1}{2}e^{-\Gamma t} - \frac{1}{2}\Phi(t)\right]\right\}, \tag{C9}$$

$$\Upsilon_8 = \eta^2\left\{d_{25}[\Phi(t) - \Theta^2(t)] + \frac{\Omega}{\Delta+\Omega}\alpha\left[\frac{1}{2}\Phi(t) + \frac{1}{2}\Theta^2(t) - \Theta(t)\Phi(t)\right]\right\}, \tag{C10}$$

$$\Upsilon_9 = \eta^2\left(d_{23}^*\{[\Theta^*(t)]^2 - \Phi(t)\} - \frac{\Omega}{\Delta-\Omega}\alpha\left\{\frac{1}{2}\Phi(t) + \frac{1}{2}[\Theta^*(t)]^2 - \Theta^*(t)\Phi(t)\right\}\right), \tag{C11}$$

$$\Upsilon_{11} = -\eta\Phi(t)[1 - \Theta(t)] + \eta^2\Phi(t)\{\Theta(t)[F(t) - F^\dagger(t)] + F(t) - F^\dagger(t)\}, \tag{C12}$$

$$\Upsilon_{12} = \eta\Phi(t)[1 - \Theta^*(t)]\eta^2\Phi(t)\{\Theta^*(t)[F^\dagger(t) - F(t)] - F(t) + F^\dagger(t)\}\,, \tag{C13}$$

$$\Upsilon_{13} = \eta^2\Phi(t)\left[\frac{1}{2}\Theta^2(t) + \frac{1}{2} - \Theta(t)\right], \tag{C14}$$

$$\Upsilon_{14} = \eta^2\Phi(t)[\Theta(t) + \Theta^*(t) - 1 - e^{-\Gamma t}], \tag{C15}$$

$$\Upsilon_{15} = \eta^2\Phi(t)\left\{\frac{1}{2}[\Theta^*(t)]^2 + \frac{1}{2} - \Theta^*(t)\right\}. \tag{C16}$$

By the same procedure, the complete time evolution for the mechanical resonator is given by

$$\begin{aligned} b(t) = {} & \Xi_0 + \Xi_1 A(0) + \Xi_2 A^\dagger(0) + \Xi_3 A^\dagger(0)A(0) + \Xi_4 b(0) + \Xi_5 b^\dagger(0) + \Xi_6 A(0)b(0) + \Xi_7 A^\dagger(0)b^\dagger(0) \\ & + \Xi_8 A^\dagger(0)b(0) + \Xi_9 A(0)b^\dagger(0) + O(\eta^3), \end{aligned} \tag{C17}$$

with Ξ_j from Eqs. (32)–(37) and the corrections

$$\Xi_1(t) = -\eta\frac{\Omega}{\Delta+\Omega}\alpha^*[e^{-\frac{\kappa}{2}t-i\phi(t)} - \Theta(t)] + \eta^2\left[2d_{25}^*\Phi(t)F_b^\dagger(t) - \left(d_{27} + \frac{\alpha^*\Delta\Omega}{\Delta^2-\Omega^2}\right)\Phi(t)F_b(t)\right], \tag{C18}$$

$$\Xi_2(t) = \eta\frac{\Omega}{\Delta-\Omega}\alpha[\Phi^*(t) - \Theta(t)] + \eta^2\left[2d_{23}^*\Phi^*(t)F_b^\dagger(t) + \left(d_{27}^* - \frac{\alpha\Delta\Omega}{\Delta^2-\Omega^2}\right)\Phi^*(t)F_b(t)\right], \tag{C19}$$

$$\Xi_6(t) = \eta^2\left\{d_{27}\Theta(t)[1-\Phi(t)] - \frac{\Omega}{\Delta-\Omega}\alpha^*\left[\frac{1}{2}\Theta(t) + \frac{1}{2}\Theta(t)\Phi(t) - e^{-\kappa t}\right] + \frac{\Omega}{\Delta+\Omega}\alpha^*\left[\Phi(t) - \frac{1}{2}\Theta(t)\Phi(t) - \frac{1}{2}\Theta(t)\right]\right\}, \tag{C20}$$

$$\Xi_7(t) = \eta^2\left\{2d_{23}^*[\Theta^*(t)\Phi^*(t) - \Theta(t)] - \frac{\Omega}{\Delta-\Omega}\alpha[\Phi^*(t) - e^{-\kappa t}]\right\}, \tag{C21}$$

$$\Xi_8(t) = \eta^2\left\{d_{27}^*[\Theta(t)\Phi^*(t) - \Theta(t)] + \frac{\Omega}{\Delta+\Omega}\alpha\left[e^{-\kappa t} - \frac{1}{2}\Theta(t) - \frac{1}{2}\Theta(t)\Phi^*(t)\right] - \frac{\Omega}{\Delta-\Omega}\alpha\left[\frac{1}{2}\Theta(t) + \frac{1}{2}\Theta(t)\Phi^*(t) - \Phi^*(t)\right]\right\}, \tag{C22}$$

$$\Xi_9(t) = \eta^2\left\{2d_{25}^*[\Theta^*(t)\Phi(t) - \Theta(t)], \frac{\Omega}{\Delta+\Omega}\alpha^*[e^{-\kappa t} - \Phi(t)]\right\}. \tag{C23}$$

[1] M. Aspelmeyer, T. J. Kippenberg, and F. Marquardt, Rev. Mod. Phys. **86**, 1391 (2014).

[2] J. Chan, T. P. M. Alegre, A. H. Safavi-Naeini, J. T. Hill, A. Krause, S. Gröblacher, M. Aspelmeyer, and O. Painter, Nature (London) **478**, 89 (2011).

[3] J. D. Teufel, T. Donner, D. Li, J. W. Harlow, M. S. Allman, K. Cicak, A. J. Sirois, J. D. Whittaker, K. W. Lehnert, and R. W. Simmonds, Nature (London) **475**, 359 (2011).

[4] S. Mancini, V. I. Man'ko, and P. Tombesi, Phys. Rev. A **55**, 3042 (1997).

[5] S. Bose, K. Jacobs, and P. L. Knight, Phys. Rev. A **56**, 4175 (1997).

[6] P. Rabl, Phys. Rev. Lett. **107**, 063601 (2011).

[7] A. Nunnenkamp, K. Børkje, and S. M. Girvin, Phys. Rev. Lett. **107**, 063602 (2011).

[8] M. Ludwig, B. Kubala, and F. Marquardt, New J. Phys. **10**, 095013 (2008).

[9] A. D. Armour and D. A. Rodrigues, C. R. Phys. **13**, 440 (2012).

[10] D. A. Rodrigues and A. D. Armour, Phys. Rev. Lett. **104**, 053601 (2010).

[11] P. D. Nation, Phys. Rev. A **88**, 053828 (2013).

[12] J. Qian, A. A. Clerk, K. Hammerer, and F. Marquardt, Phys. Rev. Lett. **109**, 253601 (2012).

[13] N. Lörch, J. Qian, A. Clerk, F. Marquardt, and Klemens Hammerer, Phys. Rev. X **4**, 011015 (2014).

[14] R. Leijssen and E. Verhagen, Nat. Sci. Rep. **5**, 15974 (2015).

[15] D. W. C. Brooks, T. Botter, S. Schreppler, T. P. Purdy, N. Brahms, and D. M. Stamper-Kurn, Nature (London) **488**, 476 (2012).

[16] S. Gröblacher, K. Hammerer, M. R. Vanner, and M. Aspelmeyer, Nature (London) **460**, 724 (2009).

[17] A. H. Safavi-Naeini, S. Gröblacher, J. T. Hill, J. Chan, M. Aspelmeyer, and O. Painter, Nature (London) **500**, 185 (2013).

[18] J. D. Teufel, D. Li, M. S. Allman, K. Cicak, A. J. Sirois, J. D. Whittaker, and R. W. Simmonds, Nature (London) **471**, 204 (2011).

[19] T. Carmon, H. Rokhsari, L. Yang, T. J. Kippenberg, and K. J. Vahala, Phys. Rev. Lett. **94**, 223902 (2005).

[20] T. Carmon, M. C. Cross, and K. J. Vahala, Phys. Rev. Lett. **98**, 167203 (2007).

[21] K. Børkje, A. Nunnenkamp, J. D. Teufel, and S. M. Girvin, Phys. Rev. Lett. **111**, 053603 (2013).

[22] M. A. Lemonde, N. Didier, and A. A. Clerk, Phys. Rev. Lett. **111**, 053602 (2013).

[23] M. A. Lemonde and A. A. Clerk, Phys. Rev. A **91**, 033836 (2015).

[24] Y.-C. Liu, Y.-F. Xiao, Y.-L. Chen, X.-C. Yu, and Q. Gong, Phys. Rev. Lett. **111**, 083601 (2013).

[25] J. R. Schrieffer and P. A. Wolff, Phys. Rev. **149**, 491 (1966).